Dalton Transactions

PAPER

View Article Online
View Journal | View Issue



Cite this: *Dalton Trans.*, 2015, **44**, 10828

# Crystal structure of A-site deficient $La_{0.2}Sr_{0.7-x}Ca_xTiO_3$ perovskite at ambient conditions and high temperatures: a neutron powder diffraction study

Ahmed D. Aljaberi[a,b] and John T. S. Irvine*[b]

Received 18th January 2015,
Accepted 4th March 2015

DOI: 10.1039/c5dt00238a

www.rsc.org/dalton

The crystal structures of several members of the solid solution perovskite $La_{0.2}Sr_{0.7-x}Ca_xTiO_3$ were investigated using the Rietveld analysis of neutron powder diffraction patterns collected in ambient conditions and high temperatures. At room temperature, samples showed a tetragonal *I*4/*mcm* symmetry for compositions with $0.1 \leq x \leq 0.35$ followed by a phase transition to the orthorhombic *Pbnm* symmetry for compositions with $0.4 \leq x \leq 0.7$. Samples with the orthorhombic symmetry showed two reversible phase transitions in the temperature range 20 °C–900 °C. The first phase transition was a discontinuous *Pbnm*–*I*4/*mcm* around 300 °C and the second was a continuous *I*4/*mcm*–$Pm\bar{3}m$ transition around 900 °C. The lower symmetries resulted from very small distortions and changes in tilts of the $BO_6$ octahedra of this perovskite material; which was a direct result from the A-site ionic radius mismatch.

## 1. Introduction

Solid oxide fuel cells are attracting much attention offering high conversion efficiency of chemical energy to electricity with an attractive possibility of using different types of fuel besides pure hydrogen. For example, methane can be used without reforming given the high operating temperature of SOFCs.[1–4] With the drawbacks of the widely used Ni-YSZ cermet anode in SOFCs,[2,5] alternative anode materials are actively being studied. These include perovskite-based materials which offer good stability during operation and tolerance to sulphur poisoning and carbon build up.[6]

Previous studies on the perovskite system $La_{0.2}Sr_{0.7-x}Ca_xTiO_3$ showed an increase in this compound's electrical conductivity with increased calcium substitution at anodic operational conditions; which was consistent with the decrease in the unit cell volume of this perovskite.[7] However, this trend was reversed at much higher calcium content; *i.e.* $x > 0.45$; which required further structural investigations of this system. Since it is widely understood that electronic conduction involves electrons on the titanium oxygen sublattices, it is anticipated that local distortions of the $TiO_6$ octahedra[8–10] can be responsible for the drop in conductivity. Due to the low scattering power of oxygen in XRD, neutron diffraction can give a better picture due to the relatively large scattering length of oxygen ions.[11]

Therefore, this paper outlines the results obtained using neutron powder diffraction to characterise the crystal structures of different compositions of the perovskite system $La_{0.2}Sr_{0.7-x}Ca_xTiO_3$ at ambient conditions, as well as, at high temperatures for the two samples discussed in previous work;[7] to investigate the origin of the slight drop in electrical conductivity.

## 2. Experimental

### 2.1 Sample preparation

Samples of $La_{0.2}Sr_{0.7-x}Ca_xTiO_3$ with $x$ = 0.1, 0.2, 0.3, 0.35, 0.4, 0.45, 0.5, 0.6 and 0.7 were synthesised using conventional solid state methods. Stoichiometric amount of high purity starting materials; *i.e.* $La_2O_3$ (Sigma-Aldrich 99.99%), $SrCO_3$ (Alfa Aesar 99%), $CaCO_3$ (Alfa Aesar 99.5%) and $TiO_2$ (Alfa Aesar 99.5%) were dried prior to weight and mixed using a mortar and pestle. All mixtures were calcined in air at 1000 °C for a minimum of 15 hours. This was followed by ball milling the powders in a planetary ball mill in acetone for 4 hours to ensure a uniform particle size. These were then dried and pressed into ~13 mm pellets using a uniaxial press. All pellets were sintered in air at 1500 °C for 15 hours. Pellets were crushed, ball milled for 4 hours and pressed, respectively, before sintering them for a second time at the same conditions. For $La_{0.2}Sr_{0.25}Ca_{0.45}TiO_3$ which showed the highest electrical conductivity of this series,[7] a pellet was reduced in a

[a]*Mechanical and Materials Engineering Department, Institute Centre for Energy – iEnergy, Masdar Institute of Science and Technology, PO Box 54224, Abu Dhabi, United Arab Emirates*
[b]*School of Chemistry, Purdie Building, University of St Andrews, St Andrews, Fife KY16 9ST, UK. E-mail: jtsi@st-andrews.ac.uk*

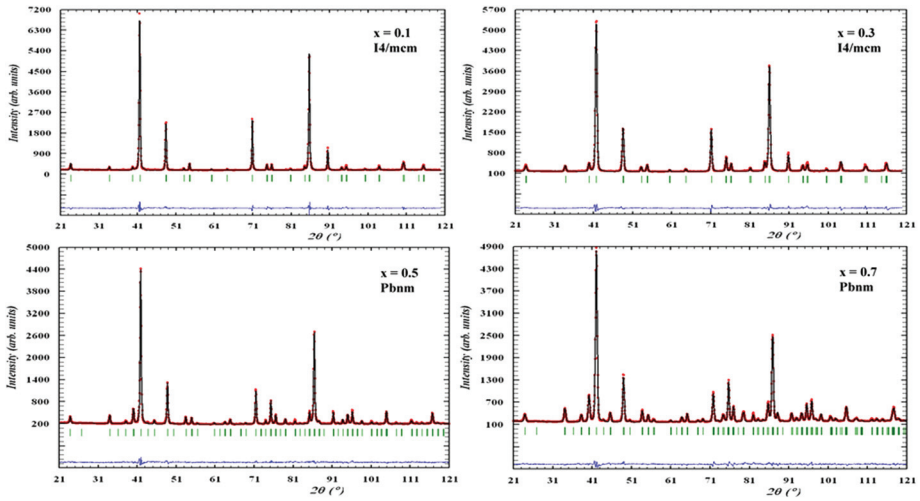


**Fig. 1** Rietveld refinement patterns for neutron diffraction data of different compositions of $La_{0.2}Sr_{0.7-x}Ca_xTiO_3$ at ambient conditions fitted to the indicated symmetries.

tube furnace at 1050 °C for 72 hours under a constant flow rate of 5% $H_2$–95% Ar gas mixture. All resulting pellets were crushed and ball milled, as above, into fine powders for neutron diffraction studies.

### 2.2 Neutron powder diffraction

Neutron powder diffraction patterns were collected using the D2B powder diffractometer at the Institute Laue-Langevin (ILL)

**Table 1** Lattice parameters, atomic positions, thermal parameters and *R*-factors from Rietveld refinement results of NPD data for the different samples of $La_{0.2}Sr_{0.7-x}Ca_xTiO_3$ at ambient conditions

| $x$ in $La_{0.2}Sr_{0.7-x}Ca_xTiO_3$ | | 0.1 | 0.2 | 0.3 | 0.35 | 0.4 | 0.45 | 0.5 | 0.6 | 0.7 |
|---|---|---|---|---|---|---|---|---|---|---|
| Space group | | *I4/mcm* | *I4/mcm* | *I4/mcm* | *I4/mcm* | *Pbnm* | *Pbnm* | *Pbnm* | *Pbnm* | *Pbnm* |
| $a$ (Å) | | 5.4918(1) | 5.4820(1) | 5.4715(1) | 5.4696(2) | 5.4652(1) | 5.4622(1) | 5.4505(2) | 5.4375(1) | 5.4221(2) |
| $b$ (Å) | | 5.4918(1) | 5.4820(1) | 5.4715(1) | 5.4696(2) | 5.4669(1) | 5.4634(1) | 5.4535(2) | 5.4463(2) | 5.4410(1) |
| $c$ (Å) | | 7.7810(2) | 7.7781(2) | 7.7544(2) | 7.7492(3) | 7.7143(1) | 7.7140(1) | 7.7013(2) | 7.6904(4) | 7.6759(3) |
| $V$ (Å$^3$) | | 234.683(7) | 233.75(1) | 232.15(1) | 231.83(1) | 230.49(1) | 230.20(1) | 228.92(1) | 227.75(2) | 226.45(1) |
| La | $x$ | 0 | 0 | 0 | 0 | −0.01(2) | −0.004(2) | 0.003(2) | 0.005(2) | 0.09(1) |
| Sr | $y$ | 0.5 | 0.5 | 0.5 | 0.5 | 0.49(2) | 0.508(1) | 0.511(1) | 0.515(1) | 0.520(1) |
| Ca | $z$ | 0.25 | 0.25 | 0.25 | 0.25 | 0.25 | 0.25 | 0.25 | 0.25 | 0.25 |
| | $B_{iso}$ (Å$^2$) | 0.34(2) | 0.52(3) | 0.42(3) | 0.33(3) | 0.16(3) | 0.46(3) | 0.51(3) | 0.42(3) | 0.49(3) |
| Ti | $x$ | 0 | 0 | 0 | 0 | 0 | 0 | 0 | 0 | 0 |
| | $y$ | 0 | 0 | 0 | 0 | 0 | 0 | 0 | 0 | 0 |
| | $z$ | 0 | 0 | 0 | 0 | 0 | 0 | 0 | 0 | 0 |
| | $B_{iso}$ (Å$^2$) | 1.051(5) | 0.791(5) | 0.445(4) | 0.790(6) | 1.119(5) | 0.625(4) | 0.488(4) | 0.763(5) | 0.266(4) |
| O1 | $x$ | 0 | 0 | 0 | 0 | −0.052(2) | −0.054(2) | −0.053(2) | −0.057(2) | −0.061(1) |
| | $y$ | 0 | 0 | 0 | 0 | 0.001(2) | −0.006(2) | −0.008(2) | −0.008(2) | −0.009(1) |
| | $z$ | 0.25 | 0.25 | 0.25 | 0.25 | 0.25 | 0.25 | 0.25 | 0.25 | 0.25 |
| | $B_{iso}$ (Å$^2$) | 0.49(5) | 0.96(6) | 1.49(5) | 1.37(6) | 1.19(6) | 0.88(5) | 0.88(5) | 0.39(6) | 0.64(8) |
| O2 | $x$ | 0.2313(1) | 0.2261(2) | 0.2206(2) | 0.2185(1) | 0.2381(1) | 0.2329(8) | 0.2291(7) | 0.2230(5) | 0.2184(4) |
| | $y$ | 0.7313(1) | 0.7261(2) | 0.7206(2) | 0.7185(1) | 0.2626(1) | 0.2691(7) | 0.2725(6) | 0.2781(5) | 0.2818(4) |
| | $z$ | 0 | 0 | 0 | 0 | 0.0227(1) | 0.0239(2) | 0.0268(3) | 0.0296(3) | 0.0317(2) |
| | $B_{iso}$ (Å$^2$) | 0.981(3) | 1.056(3) | 1.073(3) | 0.872(4) | 1.070(4) | 1.149(3) | 1.157(4) | 1.246(5) | 0.988(5) |
| *R*-Factors | $R_p$ | 3.48 | 3.68 | 3.63 | 3.75 | 3.68 | 3.35 | 2.77 | 3.42 | 3.13 |
| | $R_{wp}$ | 4.76 | 4.98 | 5.01 | 5.09 | 4.96 | 4.44 | 3.59 | 4.52 | 4.13 |
| | $R_{exp}$ | 1.95 | 1.96 | 2.02 | 1.93 | 1.86 | 1.77 | 2.01 | 1.77 | 1.92 |
| | $\chi^2$ | 5.98 | 6.42 | 6.17 | 6.95 | 7.07 | 6.33 | 3.19 | 6.48 | 4.64 |

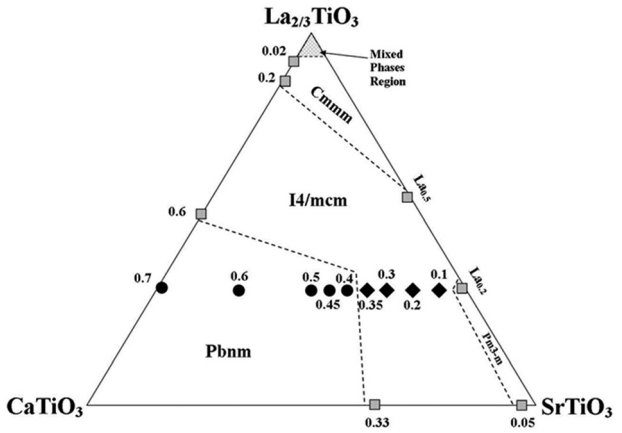


Fig. 2 Phase diagram of the ternary system $CaTiO_3$–$La_{2/3}TiO_3$–$SrTiO_3$. All numbers represent calcium content. Solid symbols represent the samples studied in this work and analysed using NPD data; where shaded ones represent compositions obtained from literature.[17–21] ◆ refers to the tetragonal samples and ● refers to the orthorhombic samples.

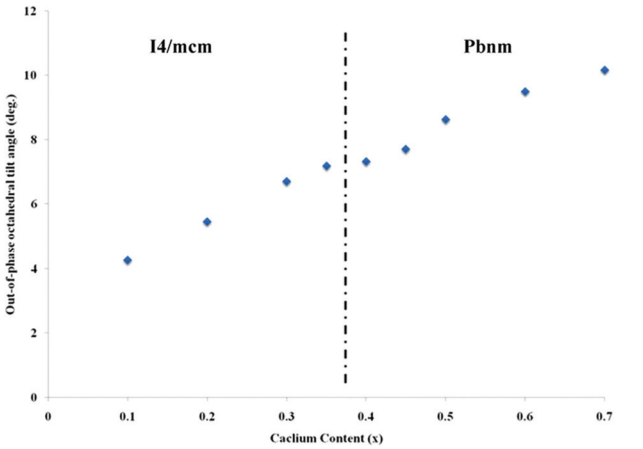


Fig. 3 The out-of-phase tilt angle values for the different compositions of $La_{0.2}Sr_{0.7-x}Ca_xTiO_3$ at room temperature.

facility in Grenoble, France. Data were collected from powder samples within vanadium containers over an angular range of $0 < 2\theta < 160°$, using a 0.05° step size, with a neutron radiation of $\lambda \approx 1.594$ Å. Data collection; *i.e.* counting time; varied between 2 hours for normal resolution and 5 hours for high resolution runs. High temperature runs were collected at various temperatures from room temperature up to 900 °C.

All patterns were analysed and refined using the Rietveld method using the software package Fullprof (version 2.05). Diffraction peaks were refined using a pseudo-Voigt function

Table 2 Lattice parameters, atomic positions, thermal parameters and *R*-factors from Rietveld refinement results of NPD data for a reduced sample of $La_{0.2}Sr_{0.25}Ca_{0.45}TiO_3$ at various temperatures

| Temperature<br>Space group | | 20 °C<br>*Pbnm* | 100 °C<br>*Pbnm* | 200 °C<br>*Pbnm* | 300 °C<br>*I4/mcm* | 500 °C<br>*I4/mcm* | 600 °C<br>*I4/mcm* | 700 °C<br>*I4/mcm* | 800 °C<br>*I4/mcm* | 900 °C<br>*Pm*$\bar{3}$*m* |
|---|---|---|---|---|---|---|---|---|---|---|
| *a* (Å) | | 5.4656(1) | 5.4720(4) | 5.4826(2) | 5.4752(1) | 5.4848(1) | 5.4960(1) | 5.5033(2) | 5.5149(8) | 3.90616(4) |
| *b* (Å) | | 5.4664(1) | 5.4743(4) | 5.4830(2) | 5.4752(1) | 5.4848(1) | 5.4960(1) | 5.5033(2) | 5.5149(8) | 3.90616(4) |
| *c* (Å) | | 7.7203(3) | 7.7263(3) | 7.7411(5) | 7.7591(4) | 7.7788(4) | 7.7934(3) | 7.8001(4) | 7.8021(2) | 3.90616(4) |
| *V* (Å$^3$) | | 230.656(1) | 231.444(3) | 232.705(2) | 232.601(2) | 234.007(1) | 235.408(1) | 236.239(2) | 237.293(8) | 59.6007(9) |
| La | *x* | −0.007(3) | −0.005(2) | −0.007(2) | 0 | 0 | 0 | 0 | 0 | 0.5 |
| Sr | *y* | 0.507(1) | 0.506(1) | 0.501(2) | 0.5 | 0.5 | 0.5 | 0.5 | 0.5 | 0.5 |
| Ca | *z* | 0.25 | 0.25 | 0.25 | 0.25 | 0.25 | 0.25 | 0.25 | 0.25 | 0.5 |
| | $B_{iso}$ (Å$^2$) | 0.56(3) | 0.74(3) | 0.92(4) | 0.99(4) | 1.37(4) | 1.61(6) | 1.87(6) | 2.09(7) | 2.25(4) |
| Ti | *x* | 0 | 0 | 0 | 0 | 0 | 0 | 0 | 0 | 0 |
| | *y* | 0 | 0 | 0 | 0 | 0 | 0 | 0 | 0 | 0 |
| | *z* | 0 | 0 | 0 | 0 | 0 | 0 | 0 | 0 | 0 |
| | $B_{iso}$ (Å$^2$) | 0.60(4) | 0.75(5) | 0.68(5) | 1.04(6) | 1.20(6) | 1.40(7) | 1.71(8) | 1.79(9) | 1.48(5) |
| O1 | *x* | −0.0523(7) | −0.0547(7) | −0.046(1) | 0 | 0 | 0 | 0 | 0 | 0.5 |
| | *y* | −0.008(1) | −0.011(1) | 0.003(3) | 0 | 0 | 0 | 0 | 0 | 0 |
| | *z* | 0.25 | 0.25 | 0.25 | 0.25 | 0.25 | 0.25 | 0.25 | 0.25 | 0 |
| | $B_{iso}$ (Å$^2$) | 1.38(8) | 1.43(8) | 1.99(9) | 2.27(7) | 1.97(7) | 1.65(9) | 1.48(9) | 1.45(8) | 3.42(2) |
| O2 | *x* | 0.2305(8) | 0.2322(1) | 0.2323(2) | 0.2174(2) | 0.2221(2) | 0.2251(2) | 0.2290(3) | 0.2353(4) | — |
| | *y* | 0.2701(8) | 0.2705(1) | 0.2617(1) | 0.7174(2) | 0.7221(2) | 0.7215(2) | 0.7290(3) | 0.7353(4) | — |
| | *z* | 0.0259(3) | 0.0238(3) | 0.0237(4) | 0 | 0 | 0 | 0 | 0 | — |
| | $B_{iso}$ (Å$^2$) | 0.95(5) | 1.06(5) | 1.37(6) | 1.74(4) | 2.46 (5) | 2.84(7) | 3.35(8) | 3.88(9) | |
| *R*-Factors | $R_p$ | 2.90 | 3.68 | 4.16 | 3.91 | 3.85 | 3.68 | 3.44 | 3.93 | 3.37 |
| | $R_{wp}$ | 3.70 | 4.67 | 5.38 | 4.97 | 4.97 | 4.71 | 4.39 | 5.05 | 4.65 |
| | $R_{exp}$ | 1.98 | 3.54 | 3.67 | 3.57 | 3.66 | 3.46 | 3.42 | 3.40 | 2.04 |
| | $\chi^2$ | 3.48 | 1.74 | 2.14 | 1.94 | 1.84 | 1.86 | 1.65 | 2.20 | 5.18 |

and the background was refined with a 6-parameter polynomial. The initial unit cell parameters were set using the findings obtained from previous XRD studies and the atomic positions for the different sites were set according to the space group symmetry.[11] B-site (Ti) atomic coordinates were kept fixed at the origin; while the other sites were allowed to vary. Occupancies were initially allowed to vary through the refinement process yielding insignificant variations from the initial stoichiometries, later these were kept fixed to nominal values to obtain more stable refinements. All models were refined to convergence with the best fits chosen by the agreement factors and stability of the refinement profiles.

# 3. Results and discussion

## 3.1 Room temperature studies

All patterns were successfully refined using the Rietveld method resulting in very good fits as shown in Fig. 1.

A significant finding of this work by using neutron diffraction was the point where the transition from the tetragonal *I*4/*mcm* to the orthorhombic *Pbnm*, see Table 1, which was previously reported to be at calcium content of $x = 0.45$.[7] The new transition point now appears to take place at a calcium content of $x = 0.4$; *i.e.* $La_{0.2}Sr_{0.3}Ca_{0.4}TiO_3$. Hence, the updated phase map of this system is shown in Fig. 2.

With neutron diffraction, there was not a strong evidence of the existence of other intermediate phases like the ones reported for the system $Ca_{1-x}Sr_xTiO_3$; *e.g. Cmmm* or *Imma*. Since the structure of the perovskite unit cell is highly affected by the A-site ionic radius mismatch, we believe that since our system incorporates a fixed stoichiometry of lanthanum; the variation of Sr/Ca ratio does not induce a severe disruption to the A-site lattice points. Thus, as it was evident from the absence of superlattice reflections in our neutron diffraction patterns that are indicative of the mentioned space groups, the system $La_{0.2}Sr_{0.7-x}Ca_xTiO_3$ undergoes a single first order phase transition with increasing calcium content; *i.e.* from *I*4/*mcm* to *Pbnm* symmetries.

Changes in symmetry in perovskites are manifested in changes to the tilt system of the $BO_6$ octahedra, which was apparent in this study. These tilt systems were analysed by having the O2 atomic coordinates as $\left(\frac{1}{4}-u, \frac{1}{4}+v, w\right)$, hence, the anti-phase tilt angle along the [001] direction in the *I*4/*mcm* phase is equal to $\varphi = \tan^{-1}4u$. The out-of-phase tilt angles along the [100] and [010] directions in the *Pbnm* phase were calculated using the relation $\varphi = \tan^{-1} 4\sqrt{2}u$.[11–13] These tilts have the Glazer notation $a^0a^0c^-$ and $a^-a^-c^+$ in the *I*4/*mcm* and *Pbnm* space groups, respectively.[14] The calculated tilt angles from the refined atomic positions for the system studied here are plotted against composition in Fig. 3.

**Table 3** Lattice parameters, atomic positions, thermal parameters and *R*-factors from Rietveld refinement results of NPD data for a reduced sample of $La_{0.2}Sr_{0.2}Ca_{0.5}TiO_3$ at various temperatures

| Temperature<br>Space group | | 20 °C<br>*Pbnm* | 300 °C<br>*I*4/*mcm* | 500 °C<br>*I*4/*mcm* | 600 °C<br>*I*4/*mcm* | 700 °C<br>*I*4/*mcm* | 900 °C<br>*Pm*$\bar{3}$*m* |
|---|---|---|---|---|---|---|---|
| *a* (Å) | | 5.4505(2) | 5.4674(2) | 5.4793(2) | 5.4874(1) | 5.4942(1) | 3.8975(1) |
| *b* (Å) | | 5.4535(2) | 5.4674(2) | 5.4793(2) | 5.4874(1) | 5.4942(1) | 3.8975(1) |
| *c* (Å) | | 7.7013(3) | 7.7447(4) | 7.7675(4) | 7.7771(3) | 7.7835(4) | 3.8975(1) |
| *V* (Å$^3$) | | 228.918(4) | 231.513(9) | 233.196(8) | 234.182(9) | 234.955(9) | 59.205(1) |
| La | *x* | 0.003(2) | 0 | 0 | 0 | 0 | 0.5 |
| Sr | *y* | 0.5107(7) | 0.5 | 0.5 | 0.5 | 0.5 | 0.5 |
| Ca | *z* | 0.25 | 0.25 | 0.25 | 0.25 | 0.25 | 0.5 |
| | $B_{iso}$ (Å$^2$) | 0.51(3) | 1.29(6) | 1.62(6) | 1.72 (6) | 1.94(6) | 2.27(8) |
| Ti | *x* | 0 | 0 | 0 | 0 | 0 | 0 |
| | *y* | 0 | 0 | 0 | 0 | 0 | 0 |
| | *z* | 0 | 0 | 0 | 0 | 0 | 0 |
| | $B_{iso}$ (Å$^2$) | 0.49(4) | 1.27(8) | 1.48(7) | 1.51(8) | 1.71(8) | 1.70(9) |
| O1 | *x* | −0.0528(7) | 0 | 0 | 0 | 0 | 0.5 |
| | *y* | −0.0079(9) | 0 | 0 | 0 | 0 | 0 |
| | *z* | 0.25 | 0.25 | 0.25 | 0.25 | 0.25 | 0 |
| | $B_{iso}$ (Å$^2$) | 0.88(6) | 2.3(2) | 1.7(1) | 1.6(1) | 1.6(1) | 3.38(5) |
| O2 | *x* | 0.2291(7) | 0.2173(2) | 0.2216(2) | 0.2236(2) | 0.2270(3) | — |
| | *y* | 0.2725(6) | 0.7173(2) | 0.7216(2) | 0.7236(2) | 0.7270(3) | — |
| | *z* | 0.0268(3) | 0 | 0 | 0 | 0 | — |
| | $B_{iso}$ (Å$^2$) | 1.16(4) | 1.63(6) | 2.52(6) | 2.81(7) | 3.24(8) | — |
| *R*-Factors | $R_p$ | 2.77 | 3.63 | 3.66 | 3.61 | 3.39 | 3.22 |
| | $R_{wp}$ | 3.59 | 4.72 | 4.64 | 4.67 | 4.39 | 4.50 |
| | $R_{exp}$ | 2.01 | 3.48 | 3.46 | 3.45 | 3.44 | 1.92 |
| | $\chi^2$ | 3.19 | 1.84 | 1.80 | 1.83 | 1.62 | 5.48 |

This result shows that our system distortions are less severe than the parent perovskite $CaTiO_3$;[12] which can be attributed to a lower A-site ionic radius mismatch, due to the fixed stoichiometry of lanthanum throughout the range of the studied compositions. This is more apparent from the almost linear change of the anti-phase tilt angle with calcium content; indicating a more stable system and re-confirms that intermediate phases are non-existing in the compositions studied here.

Calcium introduction into $SrCrO_3$ resulted in a similar behaviour to that of the system $La_{0.2}Sr_{0.7-x}Ca_xTiO_3$, in terms of structural transitions. With more calcium it was found that transitions occurred from $Pm\bar{3}m$ to $I4/mcm$ to $Pbnm$.[15]

### 3.2 High temperature studies

Two compositions; *i.e.* $La_{0.2}Sr_{0.25}Ca_{0.45}TiO_3$ and $La_{0.2}Sr_{0.2}Ca_{0.5}TiO_3$; were studied at high temperatures with the results of Rietveld refinement listed in Tables 2 and 3, respectively.

Symmetry changes were evident from the diffraction patterns as shown in Fig. 4, where both compositions showed a similar behaviour as they were orthorhombic *Pbnm* at room temperature and evolved to the ideal cubic $Pm\bar{3}m$ symmetry around 900 °C through an intermediate tetragonal $I4/mcm$ phase.

Fig. 5 and 6 show the behaviour of the lattice parameters at high temperatures of $La_{0.2}Sr_{0.25}Ca_{0.45}TiO_3$ and $La_{0.2}Sr_{0.2}Ca_{0.5}TiO_3$, respectively. These lattice parameters can be seen to discontinuously change at the *Pbnm–I4/mcm* transition point, where at the $I4/mcm$–$Pm\bar{3}m$ transition point, the lattice parameters are changing in a continuous fashion as the samples were heated. This suggests that the first transition is a first order one while the latter can be a second order or a higher phase transition. Another aspect which was observed is that this system shows the high symmetry space group $Pm\bar{3}m$ at a much lower temperature compared to that of the parent compound $CaTiO_3$, which according to Ali and Yashima[16] was found at temperatures over 1647 K. This shows that the degree of the distortion existing in $La_{0.2}Sr_{0.7-x}Ca_xTiO_3$ are much lower than those in $CaTiO_3$; which also explains the less severe distortions compared to $Sr_{1-x}Ca_xTiO_3$ as was discussed in previous publication,[7] where the A-site ionic radius mismatch is greatly affected by increasing calcium content.

Comparing between the two compositions behaviour at high temperatures, not much differences can be seen structurally. As mentioned earlier, a slight drop in electrical conductivity was seen between the two compositions at 900 °C in reducing conditions. The results here have shown a significant difference in the isotropic atomic displacement parameters between the two samples as shown in Tables 2 and 3. $La_{0.2}Sr_{0.2}Ca_{0.5}TiO_3$ showed slightly higher values at 900 °C compared to that of $La_{0.2}Sr_{0.25}Ca_{0.45}TiO_3$ especially on the titanium site. This indicates that at this temperature, the titanium atoms are less stable; *i.e.* there is mort short range disorder; on their respective atomic site within the perovskite lattice. This must translates to the extent which the conducting d-orbitals overlap; which lowers the overall electrical conductivity of this oxide. Hence, $La_{0.2}Sr_{0.25}Ca_{0.45}TiO_3$ was chosen as the optimal candidate of this series for a new type of perovskite

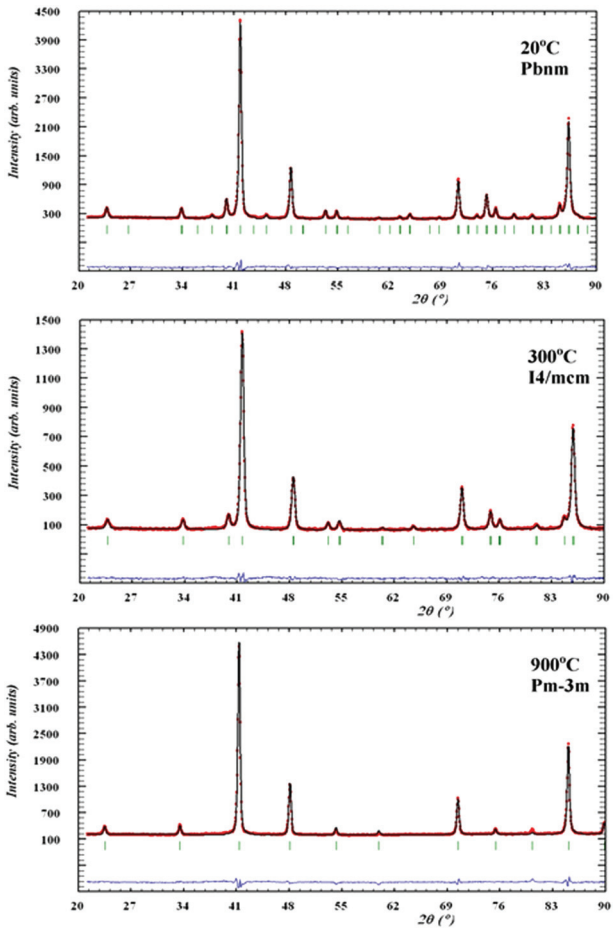


Fig. 4 Rietveld refinement of NPD patterns of a reduced sample of $La_{0.2}Sr_{0.25}Ca_{0.45}TiO_3$ at different temperatures showing the different symmetries. Note: pattern at 300 °C was collected with shorter counting time compared to the other two.

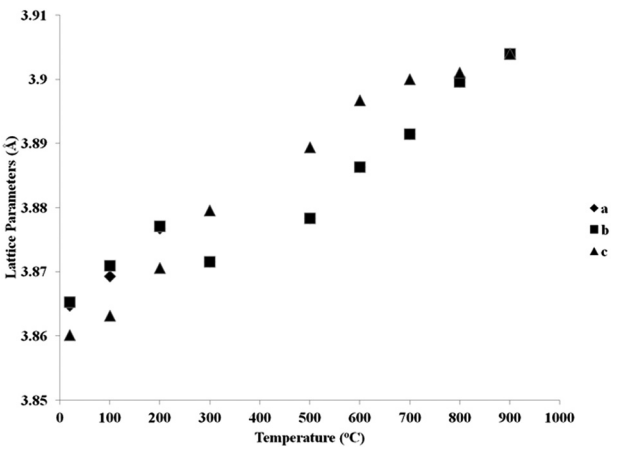


Fig. 5 Reduced lattice parameters of a reduced sample of $La_{0.2}Sr_{0.25}Ca_{0.45}TiO_3$ plotted against temperature.

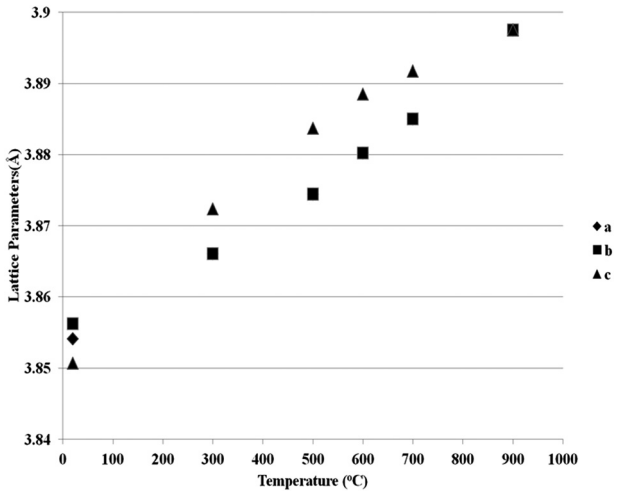


Fig. 6 Reduced lattice parameters of $La_{0.2}Sr_{0.2}Ca_{0.5}TiO_3$ plotted against temperature.

based anodes. As an anode backbone, this material is showing very encouraging performances upon further improvements.[22]

## 4. Conclusions

The perovskite $La_{0.2}Sr_{0.7-x}Ca_xTiO_3$ showed structural changes with composition and with temperature. Phase pure samples showed a drop in symmetry from the ideal cubic $Pm\bar{3}m$ of $La_{0.2}Sr_{0.7}TiO_3$ to the tetragonal $I4/mcm$ phase for $0.1 \leq x \leq 0.35$ and the orthorhombic $Pbnm$ phase for samples with $0.4 \leq x \leq 0.7$. Orthorhombic samples showed transition to higher symmetries with increasing temperature. These transitions were a discontinuous Orthorhombic $Pbnm$–Tetragonal $I4/mcm$ transitions and a continuous Tetragonal $I4/mcm$–Cubic $Pm\bar{3}m$ phase transition. These studies have helped greatly in understanding some earlier findings regarding the performance of this material as an anode material for SOFCs.

## Acknowledgements

We first thank the Government of the United Arab Emirates for sponsoring this project, the EPSRC for Platform grant support and the Royal Society for a Wolfson Research Merit Award. We also wish to thank Dr Emmanuelle Suard, ILL for her much appreciated help in collecting the neutron diffraction patterns used in this work.

## Notes and references

1 E. Lay, G. Gauthier, S. Rosini, C. Savaniu and J. T. S. Irvine, *Solid State Ionics*, 2008, **179**, 1562–1566.
2 A. Atkinson, S. Barnett, R. J. Gorte, J. T. S. Irvine, A. J. McEvoy, M. Mogensen, S. C. Singhal and J. Vohs, *Nat. Mater.*, 2004, **3**, 17–27.
3 B. C. H. Steele, *Nature*, 1999, **400**, 619–621.
4 A. Ghosh, A. K. Azad and J. T. S. Irvine, *ECS Trans.*, 2011, **35**(1), 1337–1343.
5 A. L. Sauvet and J. T. S. Irvine, *Solid State Ionics*, 2004, **167**, 1–8.
6 A. Ovalle, J. C. Ruiz-Morales, J. Canales-Vázquez, D. Marrero-López and J. T. S. Irvvine, *Solid State Ionics*, 2006, **177**, 1997–2003.
7 A. D. Aljaberi and J. T. S. Irvine, *J. Mater. Chem. A*, 2013, **1**, 5868–5874.
8 J. Zhao, N. L. Ross, D. Wang and R. J. Angel, *J. Phys.: Condens. Matter*, 2011, **23**, 455401.
9 M. Avdeev, E. N. Caspi and S. Yakovlev, *Acta Crystallogr., Sect. B: Struct. Sci.*, 2007, **63**, 363–372.
10 B. Magyari-Köpe, L. Vitos, B. Johansson and J. Kollár, *Comput. Mater. Sci.*, 2002, **25**, 615–621.
11 R. Ali and M. Yashima, *J. Solid State Chem.*, 2005, **178**, 2867–2872.
12 S. Qin, X. Wu, F. Seifert and A. I. Becerro, *J. Chem. Soc., Dalton Trans.*, 2002, **19**, 3751–3755.
13 M. A. Carpenter, C. J. Howard, K. S. Knight and Z. Zhang, *J. Phys.: Condens. Matter*, 2006, **18**, 10725–10749.
14 S. K. Mishra, R. Ranjan, D. Pandey and H. T. Stokes, *J. Phys.: Condens. Matter*, 2006, **18**, 1885–1898.
15 E. Castillo-Matinez, A. Duran and M. A. Alario-Franco, *J. Solid State Chem.*, 2008, **181**, 895–904.
16 M. Yashima and R. Ali, *Solid State Ionics*, 2009, **180**, 120–126.
17 V. Vashook, L. Vasylechko, N. Trofimenko, M. Kuznecov, P. Otchik, J. Zosel and U. Guth, *J. Alloys Compd.*, 2006, **419**, 271–280.
18 Z. Zhang, G. R. Lumpkin, C. J. Howard, K. S. Knight, K. R. Whittle and K. Osaka, *J. Solid State Chem.*, 2007, **180**, 1083–1092.
19 S. Qin, X. Wu, F. Seifert and A. I. Becerro, *J. Chem. Soc., Dalton Trans.*, 2002, 3751–3755.
20 C. J. Howard, G. R. Lumpkin, R. I. Smith and Z. Zhang, *J. Solid State Chem.*, 2004, **177**, 2726–2732.
21 T. Yamanaka, N. Hirai and Y. Komatsu, *Am. Mineral.*, 2002, **87**, 1183–1189.
22 M. C. Verbraeken, B. Iwanschitz, A. Mai and J. T. S. Irvine, *J. Electrochem. Soc.*, 2012, **159**, F757–F762.